Rayleigh Wave-Internal Wave Coupling and Internal Wave Generation Above a Model Jet Stream

B. R. Sutherland

University of Alberta, Edmonton

(Manuscript received 4 June 2004 ... *under review*)

ABSTRACT

Linear theory for modes in a non-uniformly stratified, semi-infinite shear flow demonstrates that Rayleigh waves (stable waves propagating in fluid with spatially varying shear) couple with evanescent internal waves. If the bulk Richardson number (the squared ratio of the buoyancy frequency and shear), lies between 1/4 and 1, the waves have infinite e-folding depth for waves with critical relative horizontal wavenumbers. Fully nonlinear numerical simulations examine the effect of Rayleigh-internal wave coupling when the shear layer is localised and so is Kelvin-Helmholtz unstable. Diagnostics examining profiles of the wave-induced mean flow show that if the bulk Richardson number is order unity, significant momentum is extracted from a shear layer as a consequence of transport by waves. The work is extended to the study of unstable jet flows and applications of this work for internal wave generation by dynamic instability of the upper flank of the Jet Stream are discussed.

1 Introduction

Although the most significant source of internal waves in the atmosphere is through topographic generation, other sources of internal waves are not insignificant. Particularly in the tropics, deep convective storms impinging close to the base of the stratosphere are known to excite internal waves that propagate to ionospheric heights (Fovell, Durran and Holton 1992; Alexander, Holton and Durran 1995; Walterscheid, Schubert and Brinkman 2001; Vadas and Fritts 2001; Snively and Pasko 2003). Variability associated with internal waves in the stratosphere have also been noted near the Jet Stream in the absence of topographic, convective and geostrophic adjustment sources (Herron and Tolstoy 1969; Keliher 1975; Fritts and Nastrom 1992). It is natural to suppose the source of waves is through stratified shear instability and turbulence associated with the upper flank of the Jet Stream near the tropopause. However, the detailed mechanism of wave excitation remains poorly understood.

Most investigations of shear-generation of internal waves in the atmosphere have assumed a uniform background stratification surrounding a localized shear layer. Though the most unstable mode of Kelvin-Helmholtz (KH) instability does not excite internal waves in this circumstance (Lindzen 1974; Lindzen and Rosenthal 1976), it is possible for an ensemble of modulated unstable modes to excite internal waves on scales much larger than the wavelength of the most unstable mode (Fritts 1984; Chimonas and Grant 1984; Scinocca and Ford 2000). Another possibility is that internal waves can be generated when a shear-induced mixing region collapses (Bühler, McIntyre and Scinocca 1999).

In non-uniformly stratified fluid and, in particular, for circumstances more closely resembling the upper troposphere and lower stratosphere, it is possible for internal waves on the scale of KH billows to be generated by KH instability (Sutherland, Caulfield and Peltier 1994; Sutherland and Peltier 1995; Sutherland 1996). For this to occur, the stratification over the depth of the shear layer must be sufficiently weak that the flow is indeed KH unstable. That is, the "internal" Richardson number $J_0 \equiv {N_0}^2/{S_0}^2 < 1/4$, in which N_0 and S_0 respectively are the buoyancy frequency and shear characteristic of the shear layer. One further requires that the Doppler-shifted frequency of the instability taken with respect to the flow outside the shear layer is less than the buoyancy frequency outside the shear. This amounts to requiring that the "external" Richardson number $J_1 \equiv {N_1}^2/{S_0}^2 > 1/4$, in which N_1 is the character-

Corresponding author address: Bruce R. Sutherland, Department of Mathematical and Statistical Sciences, University of Alberta, Edmonton, Alberta T6G 2G1, Canada.
Tel: (780) 492-0573; fax: (780) 492-6826.
Email: bruce.sutherland@ualberta.ca

istic buoyancy frequency outside the shear layer.

Numerical simulations have shown that when these two Richardson number criteria are met internal waves generated by KH instability are of such large amplitude and are excited for such long times that significant drag can be induced upon the mixing region (Sutherland and Peltier 1994; Sutherland 1996; Tse *et al.* 2003) and that the waves themselves can transport momentum far from the source, even across the critical layer of a second nearby stably stratified shear layer (Smyth and Moum 2002).

In section 2 we review linear theory for piecewise-linear stratified flows. We derive the dispersion relation for Rayleigh waves in an unstratified kinked-shear profile and show that resonant coupling of these waves across a finite-depth shear layer leads to KH-instability. One purpose of this paper is to extend this result to examine the coupling of Rayleigh waves with internal waves in a semi-infinite shear flow that is stratified some distance away from the shear. We then hypothesize that this coupling affects internal wave excitation from a finite-depth shear layer which is KH unstable.

It is computationally infeasible and indeed unrealistic to simulate the nonlinear evolution of a non-uniformly stratified semi-infinite shear flow. However, the simulations of a shear layer presented in section 3 clearly demonstrate a transition from direct wave excitation by internal wave-Rayleigh wave coupling to indirect excitation by flow over well-developed KH billows.

We further extend the simulations to model wave excitation from a non-uniformly stratified jet flow in which the lower flank of the jet is marginally stable and the upper flank is unstable in the sense that $J_0 < 1/4$. A range of simulations are performed to estimate the relative loss of momentum from the jet as a function of the distance to and strength of the enhanced stratification above the jet.

Implications of this work for internal wave generation by dynamic instability of the Jet Stream are discussed in section 4.

2 Theory

We begin this section with a brief review of well known results from linear stability theory for piecewise-linear velocity profiles in unstratified and stratified fluid. We then examine the coupling of Rayleigh waves with internal waves.

a Rayleigh Waves and Kelvin-Helmholtz Instability

Consider an unbounded, inviscid, uniform fluid with a semi-infinite shear flow profile given by

$$\bar{U} = \begin{cases} 0 & z \geq 0 \\ S_0 z & z < 0. \end{cases} \tag{1}$$

Such a kinked-shear flow supports neutrally propagating Rayleigh waves (*e.g.* see Drazin and Reid 1981 §23, Caulfield 1994), which satisfy the following dispersion relation given in nondimensional form:

$$\omega = -S_0/2. \tag{2}$$

The horizontal phase speed of the waves varies inversely with their horizontal wavenumber, k, according to

$$c = -S_0/(2k). \tag{3}$$

A finite-depth shear layer given by

$$\bar{U} = \begin{cases} -U_0 & z \geq L \\ S_0 z & |z| < L, \\ U_0 & z \leq -L \end{cases} \tag{4}$$

with $S_0 = -U_0/L$, is KH unstable. The instability occurs because Rayleigh waves on either flank of the shear resonantly couple, growing in amplitude at the expense of energy drawn from the mean flow (Caulfield 1994,Baines and Mitsudera 1994). The coupled waves satisfy the dispersion relation given in nondimensional form by

$$\tilde{\omega}^2 = \frac{1}{4}\Big[(1-2\tilde{k})^2 - e^{-4\tilde{k}}\Big], \tag{5}$$

in which we have defined $\tilde{k} \equiv kL$ and $\tilde{\omega} \equiv \omega/S_0$. If $0 < \tilde{k} \lesssim 0.64$, $\tilde{\omega}$ is a pure imaginary number whose magnitude is the growth rate of the instability. The fastest growing mode occurs for $\tilde{k}^\star \simeq 0.398$, for which the growth rate is $\tilde{\omega}_i^\star \simeq 0.20$ (*e.g.* see Drazin and Howard 1966 §II). The frequency of this mode is zero, meaning the wave has the same horizontal phase speed as the shear layer at mid-depth (at $z = 0$). In a frame of reference moving with the speed of the fluid above $z = L$, the nondimensional (Doppler-shifted) frequency of this mode is $\tilde{\Omega}^\star \equiv \Omega/S_0 = \tilde{k}^\star \simeq 0.398$.

In uniformly stratified fluid characterized by constant buoyancy frequency, N_0, the shear layer given by (4) is unstable if the (internal) Richardson number $J_0 = {N_0}^2/{S_0}^2 < 1/4$ (Miles 1961,Drazin and Howard 1966). As J_0 increases from 0 to 1/4, the wavenumber and (real) frequency of the most unstable mode hold approximately constant values, while the growth rate decreases monotonically to zero.

b Rayleigh Wave-Internal Wave Coupling

Now consider the semi-infinite shear flow prescribed by (1) in a non-uniformly stratified fluid characterized by squared buoyancy frequency

$$N^2 = \begin{cases} {N_1}^2 & z \geq H \\ 0 & z < H. \end{cases} \tag{6}$$

We require bounded solutions and, for cases in which propagating waves exist above $z = H(\geq 0)$, we require causality so that the waves move upward. Thus we assume the streamfunction amplitude, $\hat{\psi}(z)$, is represented by

$$\hat{\psi} = \begin{cases} Ae^{-\gamma z} & z \geq H \\ B_1 e^{kz} + B_2 e^{-kz} & 0 \leq z < H \\ Ce^{kz} & z < 0, \end{cases} \tag{7}$$

in which

$$\gamma = k\sqrt{1 - \frac{{N_1}^2}{(ck)^2}}. \tag{8}$$

Generally, c may be complex-valued. To require boundedness and to filter waves that propagate inward from infinity (*e.g.* see Scorer 1949), the branch cut for γ is defined so that the real part of the square root is non-negative and pure imaginary roots lie on the positive imaginary axis. That is, if c is real and $ck < N_1$, then $\gamma = \imath k({N_1}^2/(ck)^2 - 1)^{1/2}$.

Vertical velocity and pressure continuity require that $\hat{\psi}$ is continuous and differentiable at $z = 0$ and $z = H$. The resulting set of four equations in unknowns A, B_1, B_2 and C is an eigenvalue problem. Explicitly, we find that the nondimensional frequency $\tilde{\omega}$ must be related to the nondimensional horizontal wavenumber $\hat{k} \equiv kH$ and external bulk Richardson number $J_1 \equiv {N_1}^2/{S_0}^2$ through the roots of the cubic polynomial

$$\tilde{\omega}^3 + \frac{1}{2}\tilde{\omega}^2\left(1 + J_1 e^{2\hat{k}}\right) + \frac{1}{2}J_1\tilde{\omega}\left(e^{2\hat{k}} - 1\right) + \frac{1}{2}J_1 \sinh^2(\hat{k}). \tag{9}$$

In the case $J_1 = 0$ we recover the dispersion relation for Rayleigh waves together with two zero roots. For J_1 positive, the root corresponding to Rayleigh waves continues to be real valued. The two zero roots split to give complex-conjugate valued frequencies for a range of H. However, this pair of roots is unphysical: for all positive J_1, they correspond to modes for which the real part of γ is negative and hence, to waves that have unbounded amplitude as $z \to \infty$. The Boussinesq approximation precludes the existence of such waves.

If $H = 0$, the root corresponding to Rayleigh waves moving in the presences of a semi-infinite stratified layer has dispersion relation $\tilde{\omega} = -(J_1 + 1)/2$. The magnitude of the wave frequency relative to the buoyancy frequency is

$$\frac{|\omega|}{N_1} = \frac{|\tilde{\omega}|}{\sqrt{J_1}} = \frac{1}{2}\left(\sqrt{J_1} + \frac{1}{\sqrt{J_1}}\right)$$

This has minimum value if $J_1 = 1$ in which case $|\omega|/N_1 = 1$. For all other J_1, the frequency exceeds the buoyancy frequency above $z = 0$ and so only evanescent internal waves are excited by Rayleigh waves. The structure of waves when $J_1 = 1$ are "marginal modes" in the sense that they are neither evanescent (with finite e-folding depth) nor vertically propagating (with pure imaginary γ). As such, γ is identically equal to zero for marginal modes.

Generally, for non-negative $\hat{k}$ we find Rayleigh waves couple with evanescent internal waves with finite e-folding depth except at a single value of J_1 for which $|\omega| = N_1$. The value of J_1 for which this occurs is given by

$$J_1 = \frac{1}{4}\left(1 + e^{-2\hat{k}}\right)^2, \tag{10}$$

and is plotted in Fig. 1a. Given J_1, we define marginal Rayleigh-internal (RI) modes to be waves with nondimensional wavenumber $\hat{k}$ satisfying (10) and, hence, with infinite e-folding depth in the upper half-plane. Note that marginal RI modes may be excited only if J_1 lies between 1/4 and 1.

The vertical structure of two representative marginal RI modes is plotted in Fig. 1b. With respect to an arbitrary length scale we plot these curves corresponding to a mode with horizontal wavenumber $k = 0.4$ (a value that will be considered in the discussion below) in stratified fluid for which $H = 0$ ($\hat{k} = 0$ and $J_1 = 1$) and $H = 3$ ($\hat{k} = 1.2$ and $J_1 \simeq 0.30$).

For J_1 between 1/4 and 1, there is a single value of $\hat{k}$, given by (10), for which the the relative amplitude of marginal RI mode in the far-field is constant. The value of this constant is decreases as H increases. For other values of $\hat{k}$ or for J_1 outside the range $[1/4, 1]$, the the far-field disturbance decays exponentially with height.

In the discussion so far, we have focused upon marginal RI modes because these have substantial far-field influence. Likewise, for given J_1, modes with $\hat{k}$ close to that of the corresponding marginal RI mode create disturbances far above the shear. Next we consider how such modes might connect with unstable KH modes to excite vertically propagating waves.

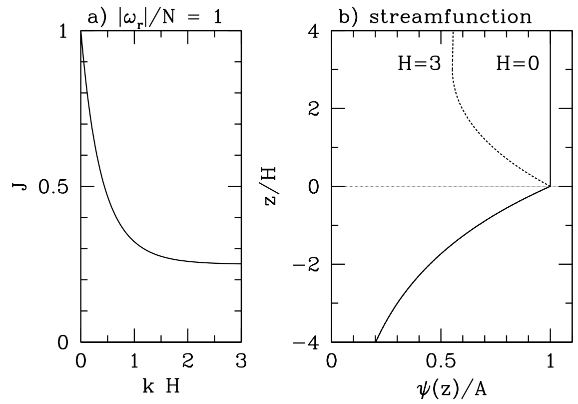

Figure 1: a) Marginal curve for internal wave generation represented by the bulk Richardson number, $J \equiv {N_1}^2/{S_0}^2$, as a function of nondimensional wavenumber, $\hat{k} \equiv kH$. b) Streamfunction amplitude of marginal modes with $H = 0$ (solid line) and $H = 3$ (dotted line) measured in arbitrary spatial units. In both cases $k = 0.4$ and the function is normalised so that its maximum value is unity. Note, the imaginary part of ψ is zero for all z.

c Internal Wave Excitation by KH Instability

The stability problem for the piecewise-linear shear layer, (4), having a uniformly stratified fluid above, given by (6), requires finding the roots of a quintic polynomial. Rather than do this explicitly, we gain insight into the interaction between KH and RI modes by examining the problems separately. The key nondimensional parameters in this study are $\delta \equiv H/L$, the ratio of the height of the stratified region above the shear layer to the half-depth of the layer, and the external bulk Richardson number $J_1 \equiv {N_1}^2/{S_0}^2$. For simplicity of this discussion, we assume the fluid is unstratified over the depth of the shear layer. Because the gradient Richardson number is less than 1/4, KH instability occurs. If the stratification above is sufficiently large, internal waves may also be excited through either of two generation mechanisms.

In one, the "indirect mechanism", the fluid is stratified sufficiently far above the shear layer ($\delta \gg 1$) that KH instability develops being only weakly influenced by the far-field stratification. Consequently the flow passing over the growing shear unstable waves and the nonlinearly developed billows moves up and down similar to flow moving over periodic topography. Provided the stratification is sufficiently strong and not too far above the billows, internal wave generation should occur in a manner similar to topographic wave generation (Sutherland 1996). Specifically, because the nondimensional frequency of the most unstable KH mode taken with respect to the far field is $\tilde{\Omega}^\star \simeq 0.40$, then propagating waves are excited if $J_1 \gtrsim 0.16$.

In a second ("direct") mechanism for internal wave excitation, the fluid is stratified close to the shear layer ($0 \leq \delta \ll 1$) and so the stratified region is significantly disturbed even during the initial growth phase of the KH instability. Because the flow is unstable the far-field disturbance will exhibit vertical oscillations within an envelope having exponentially decreasing amplitude (Sutherland, Caulfield and Peltier 1994). (For example, if ω, and hence c, is complex-valued in (8), then γ must likewise be complex-valued.)

In light of the discussion above on Rayleigh-internal wave coupling, we anticipate the disturbance will extend farthest above the shear layer if $1/4 \leq J_1 \leq 1$ and if the nondimensional horizontal wavenumber corresponding to the most unstable KH mode, $\hat{k}^\star = \tilde{k}^\star\delta \simeq 0.40\delta$, approximately satisfies (10). In particular, the strongest coupling should occur if $\delta = 0$ and $J_1 = 1$. Because the frequency of the most unstable KH mode is less than the frequency of RI-modes, direct resonant coupling does not occur. Such modes may be excited nonetheless by the transient growth of the KH instability.

These two generation mechanisms are examined in the numerical simulations that follow.

3 Numerical Simulations

Though linear theory usefully assesses under what circumstances internal waves are dynamically generated in a non-uniformly stratified shear flow, fully nonlinear simulations are necessary to determine whether internal waves continue to be excited after the modes grow to large amplitude. Here we show wave emission from a shear layer is indeed long-lived and that the momentum extracted from the shear by the waves is so large that the evolution of the shear is significantly modified. We further examine the evolution of a jet flow whose upper flank is unstable, just as in the simulations of the shear layer, but whose lower flank is dynamically stable. These latter simulations more closely represent the short-time evolution of a dynamically unstable Jet Stream underlying the stratosphere.

a The model

We solve the fully nonlinear Navier-Stokes equations in two-dimensions using a mixed finite-difference, spectral code (Sutherland and Peltier 1994). The equations are simplified by invoking the Boussinesq approximation which, although it filters anelastic effects, is reasonable to apply here because the phenomena of wave generation by dynamic instability of the Jet Stream occurs on 1 km length-scales, smaller than the scale height of the atmosphere at the altitude of the tropopause. As a consequence, it is sufficient for us to use density rather than potential temperature as a basic state variable in our equations. For numerical stability, it is necessary to introduce viscosity. However, the Reynolds number of the flow is set to be sufficiently large (typically 1000 based on the flow speed and shear depth) that the dynamics of instability and wave generation are not significantly influenced by viscous effects.

Length- and time-scales in the simulations are set by the depth and strength of the shear flow immediately below the stratified region. We thereby prescribe the background velocity profile in nondimensional form:

$$\bar{U} = \left\{ \begin{array}{cl} -1 & z \geq 1 \\ -z & |z| < 1 \\ 1 & -L_w \leq z \leq -1 \\ \frac{z-1-L_w-L_b}{L_b} & |z-1-L_w-L_b| < L_b \\ -1 & z \leq -1-L_w-2L_b. \end{array} \right. \tag{11}$$

Generally, this is a piecewise-linear jet flow in which the shear layer on the upper flank has half-depth 1 and the shear layer on the lower flank has half-depth L_b. The vertical extent of the jet is set by L_w. In the limit $L_w \to \infty$, this becomes the shear layer profile given by (4) with $U_0 = L = 1$.

The background density profile is represented by the squared buoyancy frequency

$$N^2 = \left\{ \begin{array}{ll} J_1 & z \geq 1+\delta \\ J_0 & z < 1+\delta, \end{array} \right. \tag{12}$$

in which δ is the nondimensional distance between the top of the jet and the region of enhanced stratification.

Figure 2 plots these background profiles used in a typical simulation. In all simulations we restrict $L_b = 5$ and $J_0 = 0.01$ so that the bottom flank of the jet is marginally stable in the sense of the Miles-Howard criterion (Miles 1961; Howard 1961) that the gradient Richardson number locally equals 1/4. Simulations are performed that examine the effect of varying L_w, δ and J_1.

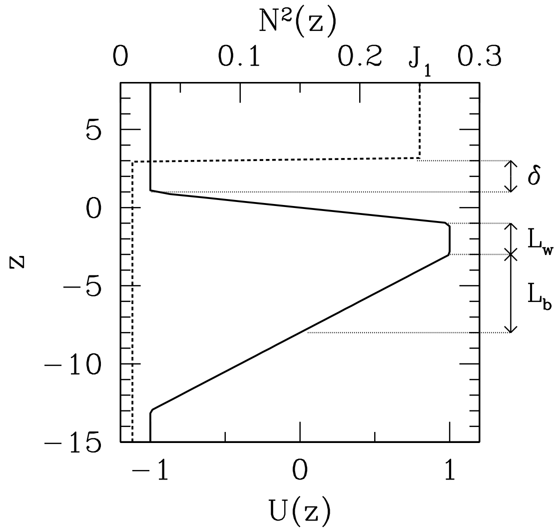

Figure 2: Initial background velocity (solid line, with corresponding axis at bottom of graph) and squared buoyancy frequency profiles (dashed line, with corresponding axis at top of graph). Both profiles are given in nondimensional form by setting $U_0 = L = 1$. In these plots, the velocity is given by eq. (11) with $L_w = 2$ and $L_b = 5$, and the buoyancy frequency is given by eq. (12) with $\delta = 2$, $J_0 = 0.01$ and $J_1 = 0.25$.

The computational domain is horizontally periodic and is bounded vertically with free-slip boundaries at $z = -40$ and 100. This vertical extent is chosen so that boundaries are so far from the shear layer that they insignificantly affect the instability and wave generation dynamics. The horizontal extent is $L_x = 2\pi/0.41 \simeq 15.3$, large enough to accommodate one wavelength of the most unstable KH mode.

The wavenumber and structure of the most unstable mode is determined by a Galerkin analysis (Klaassen and Peltier 1985) that includes the effects of diffusion on the growth of the most unstable mode. The fact the growth rate and wavelength of the most unstable mode differ by less than 2 percent of those predicted by inviscid linear theory is confirmation that diffusion does not play a significant role in the observed dynamics. The most unstable mode is superimposed on the background flow with its amplitude set so that its associated maximum vertical velocity is initially 0.01. We superimpose small amplitude noise in higher modes.

The horizontal and vertical resolution of the simulations is 0.07 and time steps are advanced in increments of 0.005. The simulations are run up to time $t \equiv t_f = 100$. This is sufficiently long that the instability develops and waves are generated but not so long that the waves reach the vertical boundaries of the domain. As well as boundary influences, simulations are not run for longer times because realistically the mixing region would not remain two dimensional and so wave generation by shear instability would be poorly represented after a few turnover times (Peltier and Caulfield 2003).

b *Wave-induced Mean Flow Analysis*

The generation of internal waves and their effect upon the mixing region are diagnosed by examining horizontally averaged horizontal flow, $\langle u \rangle$, as it evolves over time and also by examining profiles of $\langle \zeta\xi \rangle$. The latter expression is the horizontal average of the product of the vorticity and vertical displacement field. To second-order accuracy, it is identical to the wave-induced mean flow (the pseudomomentum per unit mass) due to internal waves in non-overturning regions (Scinocca and Shepherd 1992; Sutherland 1999; Sutherland 2001). Accordingly, the conservation of pseudomomentum for a two-dimensional Boussinesq fluid dictates that

$$\frac{\partial}{\partial t} \langle \zeta\xi \rangle = -\frac{\partial}{\partial z} \langle uw \rangle . \qquad (13)$$

That is, the wave-induced mean flow changes in time due to the divergence of the Reynolds stress per unit mass, $\tau/\rho_0 = \langle uw \rangle$.

Typically, momentum transport is represented by the Reynolds stress, which measures the vertical transport of horizontal momentum and, consequently, the drag imparted to the mean flow. In particular, the average decrease in the momentum of the mean flow between two fixed levels, z_1 and z_0, respectively above and below the mixing region, can be computed by finding the integral over time of $\tau(z_1) - \tau(z_0)$ and dividing by $z_1 - z_0$. This calculation requires knowing the momentum flux as a function of time. The result is also dependent upon the choice of both z_0 and z_1.

We instead diagnose the loss of momentum from the mixing region from the wave-induced mean flow, $\langle \zeta\xi \rangle$. To second order accuracy, the law of conservation of pseudomomentum predicts that $\partial \langle \zeta\xi \rangle / \partial t$ equals the divergence of the Reynolds stress per unit mass, $\langle uw \rangle$ (Scinocca and Shepherd 1992). Thus, as we demonstrate below, working with $\langle \zeta\xi \rangle$ has the advantage that its profile at a fixed time allows one to compute the cumulative momentum extracted from the mean flow by waves. Therefore momentum transport can be diagnosed from instantaneous fields rather than from time series. From this, the time-averaged Reynolds stress due to wave emission can be computed. The result is expressed in a form that depends only upon z_1 and not z_0.

c *Shear Flow Results*

Figure 3 shows a snapshot at time t_f of a piecewise-linear shear layer ($L_w \to \infty$ in (11)) that has evolved nonlinearly in three different simulations. In Fig. 3a the initial state is prescribed by a background of uniformly stratified fluid such that $J_1 = J_0 = 0.01$. Figs. 3b and c show the results of simulations of non-uniformly stratified fluid with $J_1 = 1$ and with $\delta = 3$ and 1, as indicated.

In all three cases, the leftmost panels show contours of the vorticity field over a portion of the full vertical extent of the computational domain. The plots reveal both the development of a negative-signed coherent vortex in the mixing region and the generation of large amplitude internal waves in the non-uniformly stratified simulations.

Analysis of the power spectra of the waves for a wide range of simulations reveals that the magnitude of the ratio of the vertical to horizontal wavenumber increases approximately as the square root of J_1 as J_1 becomes large. This is consistent with linear theory for waves with fixed horizontal wavenumber and frequency. Though small in amplitude to this extent, the cumulative effect of wave excitation has a significant influence upon the mean flow. In particular, movies of the simulations shown in Fig. 3 reveal that the vortex, once it develops, is stationary in the uniformly stratified case but moves leftward in the two non-uniformly stratified cases.

An explanation for this motion is made apparent by examining the centre panels, which compare profiles of $\langle u \rangle$ at time t_f with the initial background mean-flow profile. In the uniformly stratified case, mixing redistributes momentum about the mid-depth of the shear layer, but the horizontal flow remains symmetric about $z = 0$. However, the $\langle u \rangle$ profile is not symmetric in simulations in which waves are generated. Indeed the mean flow accelerates substantially well above the shear layer as a result of momentum transport by waves. The mean flow associated with the shear layer itself is significantly modified as a consequence both of mixing and momentum extraction by waves. In particular, the mean depth of the shear drops below $z = 0$ and so the flow at $z = 0$ becomes negative. Thus the vor-

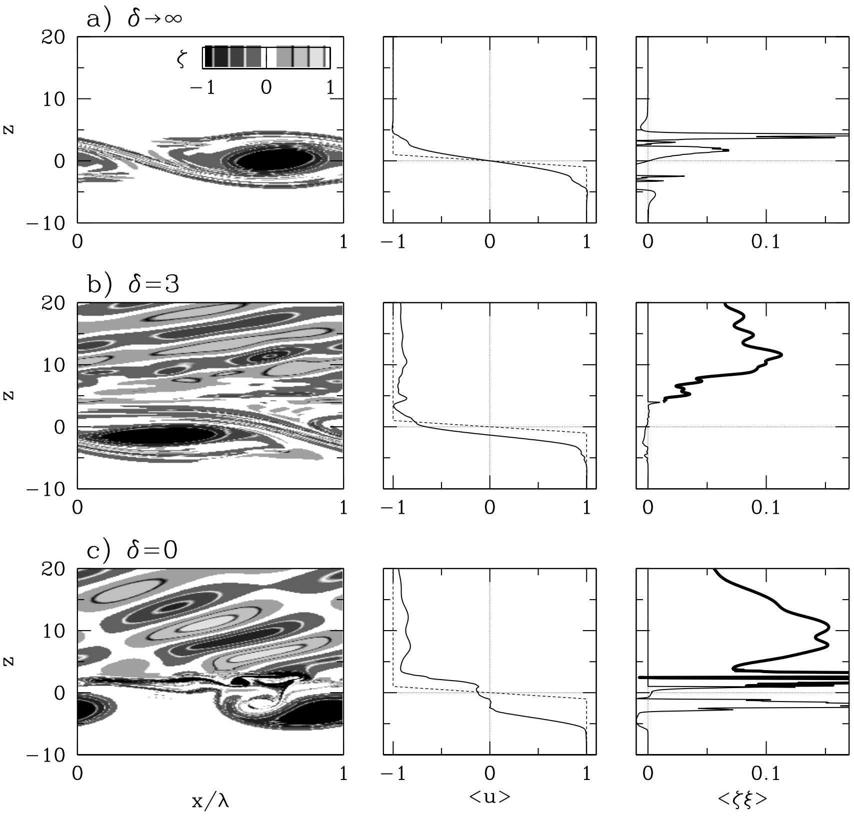

Figure 3: Diagnostics at time $t = 100$ from simulated evolution of piecewise linear shear in a) uniform stratification $J_0 = 0.01$, and in nonuniform stratification with $J_0 = 0.01$ below $z = \delta$ and $J_1 = 1$ above $z = \delta$ in which b) $\delta = 3$ and c) $\delta = 0$. In all three circumstances, the left-hand contour plots show the vorticity field ζ on the scale given in the inset of the vorticity plot in a). The middle plots show the mean horizontal flow at $t = 0$ (dashed line) and at $t = 100$ (solid line). The right-hand plots show the profiles of $\langle\zeta\xi\rangle$ drawn with thin lines below $z = \delta$ and with thick lines above $z = \delta$. Sufficiently far above $z = \delta$ values of $\langle\zeta\xi\rangle$ are meaningfully interpreted as the wave-induced mean flow.

tices move leftward because internal wave generation results in a substantial drag to the mean flow.

Figure 4 shows the early time evolution of vertical profiles of the momentum flux per unit mass during early times in 6 simulations. The values of $\langle uw\rangle$ are plotted with a logarithmic grayscale so that contours which are evenly spaced horizontally correspond to exponential growth in time. Such evenly spaced contours are expected during the initial linear growth phase of the instability.

In Figs. 4a and c, $\delta = 0$. Thus the nondimensional wavenumber $\hat{k}$, as defined above (9), is zero and therefore, according to (10), direct wave excitation through coupling with marginal RI modes occurs if $J_1 = 1$. Indeed, Fig. 4a shows that momentum transport by waves is initiated immediately during the linear growth phase of the unstable mode when $J_1 = 1$. The momentum flux grows exponentially near $z = 0$, at the midpoint of the shear, and grows to increasingly large heights in the stratified region above the shear layer. This latter growth is associated with transport by internal waves. Because the amplitude of the unstable mode changes smoothly from the shear layer to the stratified region above, wave generation plays as an important role in driving the instability as does the shear layer itself: the wave generation mechanism is direct.

In the other three simulations shown in Fig. 4c, the momentum transport takes place in two stages. As the shear instability develops, $\langle uw\rangle$ grows exponentially about $z = 0$ and then grows in the stratified region above $z = 1$ after a time delay. Because the contours are evenly spaced horizontally the shear instability and consequent wave radiation are apparently coupled during the initial linear growth phase. Compared with Fig. 4a, the closer packing of the

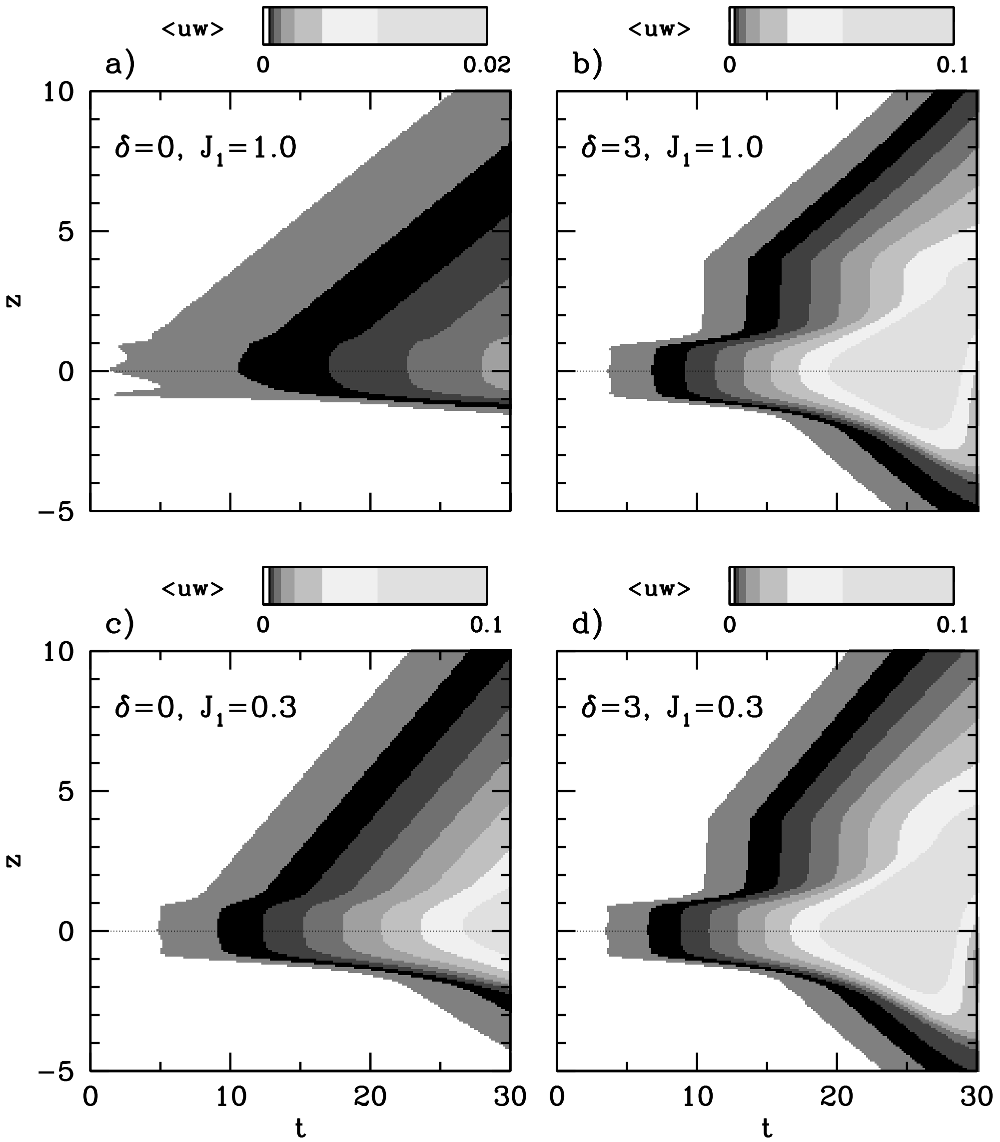

Figure 4: Time series showing contours of Reynolds stress per unit mass, $\langle uw \rangle$, in four shear flow simulations with parameters δ and J_1 as indicated.

contours in Figs. 4b-d reflects the relatively faster growth rate of the corresponding unstable modes.

The time delay for the growth of disturbances above $z = 1 + \delta$ indicates that it is primarily the shear flow that drives the instability. The momentum flux due to waves being that much smaller above the shear layer means that wave generation does not play an active role in the instability: the generation mechanism is indirect. At later times, particularly in simulations with sufficiently large δ, nonlinear effects lead to the development of a vortex in the shear layer, and this coherent disturbance acts further to excite waves.

Thus the simulations demonstrate that the direct generation mechanism operates only for $\delta \simeq 0$ and $J_1 \simeq 1$.

Over the duration of a simulation, the amount of drag can be quantified by examining the wave-induced mean flow from profiles of $\langle \zeta\xi \rangle$. These are plotted in the rightmost panels of Fig. 3. Thin lines are drawn below $z = 1+\delta$ over the depth of the mixing region and thick lines are drawn above $z = 1+\delta$. Above $1+\delta$ the field is dominated by waves and $\langle \zeta\xi \rangle$ can be interpreted as the wave-induced mean flow.

Of the two simulations with non-uniformly stratified fluid, the magnitude and extent of the wave-induced mean flow profile is larger in the case $\delta = 0$, for which the stratified region directly overlies the shear layer. Even after the initial linear phase of growth, internal wave transmission continues to be strong for long times. This occurs in part because the vortex in the mixing region acts an obstacle over which the stratified region flows and thereby generates waves in a manner similar to stratified flow over topography. The closer the obstacle to the region, the stronger the wave excitation.

We quantify the effect of internal wave transmission on the evolution of the mixing region by assessing the momentum transported by waves and the consequent displacement and spreading of the mean flow.

The vertical integral of $\langle\zeta\xi\rangle$ over the extent of the wave region gives the loss of momentum per unit mass to the mean flow due to momentum transport by waves. Explicitly we define

$$\Delta M \equiv \int_{z_c}^{\infty} \langle\zeta\xi\rangle\; dz, \tag{14}$$

in which we set $z_c = 7$. This value of z_c is chosen to be sufficiently far above the mixing region in all simulations that $\langle\zeta\xi\rangle$ well represents the wave-induced mean flow but the value is sufficiently close to the mixed region that the wave field exists predominantly above z_c. A direct numerical check confirms that the difference between $\langle u\rangle$ at time $t = t_f$ and $t = 0$ differs from the value of $\langle\zeta\xi\rangle$ at t_f by less than 0.1% over the vertical extent of the wave-dominated region.

In order to relate ΔM to the momentum loss from the mixing region, we define $\Delta z_{\rm igw}$ to be the decrease in mean depth of the shear layer as a result of drag due to wave emission. That is, $\Delta z_{\rm igw}$ is defined implicitly by $\int_{-\infty}^{\infty} \bar{U}(z-\Delta z_{\rm igw}) - \bar{U}(z)\, dz = \Delta M$, in which $\bar{U}(z)$ is the initial background velocity profile. Explicitly, this requires

$$\Delta z_{\rm igw} = -\Delta M/2 \tag{15}$$

An alternate representation of the momentum loss due to wave emission is derived by comparing profiles of

$$\hat{U} \equiv \begin{cases} \langle u\rangle - \langle\zeta\xi\rangle & z \geq z_c \\ \langle u\rangle & z < z_c \end{cases} \tag{16}$$

at the start and end of a simulation. By subtracting the wave-induced mean flow above z_c from the horizontally averaged flow, $\hat{U}$ represents the redistribution of momentum primarily due to mixing not wave transport. We quantify this redistribution by computing the mean depth, μ, of the background shear, $d\hat{U}/dz$:

$$\mu \equiv \int \left(z\frac{d\hat{U}}{dz}\right) dz \Big/ \int \left(\frac{d\hat{U}}{dz}\right) dz. \tag{17}$$

Finally, we define

$$\Delta z_{\rm shr} \equiv \mu\big|_{t=t_f} - \mu\big|_{t=0}, \tag{18}$$

which measures the decrease in the mean depth of the shear over the course of the simulation.

For a wide range of simulations we find that $\Delta z_{\rm igw} \simeq \Delta z_{\rm shr}$ to better than 99.9% accuracy. This confirms that wave emission accounts for the extraction of momentum from the mean shear.

From these diagnostics we may estimate the average Reynolds stress, τ, acting over a distance $\Delta z_{\rm shr}$ for the duration t_f of the simulation. Explicitly,

$$\tau \simeq -\rho_0\,(2U_0/t_f)\,\Delta z_{\rm shr}, \tag{19}$$

in which ρ_0 is the characteristic density at mid-depth of the shear layer. (This Boussinesq form is suitable even for atmospheric applications provided the depth of the shear layer is much less than the density scale height.)

The second method of measuring the momentum loss has the added advantage that it also provides an estimate of mixing in the shear layer. We define σ to be standard deviation of the distribution represented by the background shear, $d\hat{U}/dz$. We then define

$$\Delta\sigma = \frac{\sigma\big|_{t=t_f} - \sigma\big|_{t=0}}{\sigma\big|_{t=0}}, \tag{20}$$

which represents the increase in depth of the shear layer due to mixing taken relative to the half-depth of the initial shear.

In the control simulation with $J_1 = J_0 = 0.01$ ($\delta \to \infty$), $\Delta z_{\rm shr} = 4\times 10^{-4}$. This small value is consistent with the observation that momentum is redistributed about $z = 0$ but the mean depth of the shear layer does not drop when internal waves are not significantly excited. In this case we find $\Delta\sigma = 0.6$, indicating that mixing acts only moderately to redistribute momentum about the initial region of maximum shear.

The impact of wave transmission upon the evolution of the shear layer is examined for a wide range of simulations in Figure 5. From simulations with $\delta = 3$ and varying J_1, Fig. 5a shows that the depth of the shear layer broadens moderately and the mean depth of the shear layer decreases as a consequence

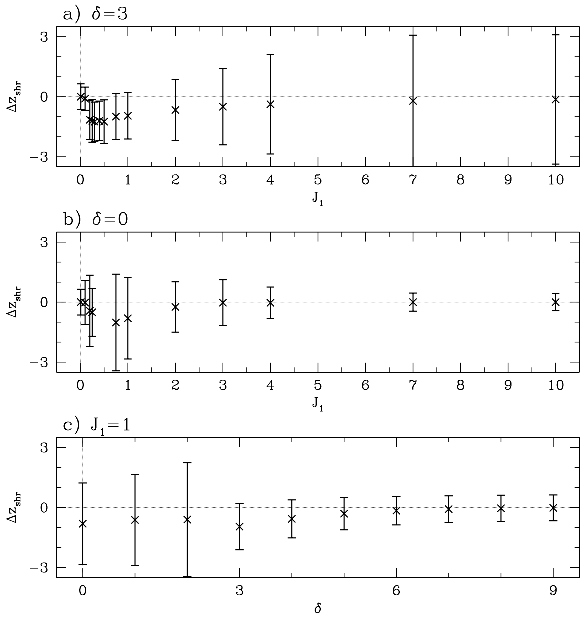

Figure 5: The displacement, $\Delta z_{\rm shr}$ (crosses), and the spread, $\Delta\sigma$ (vertical bars), of the mixing region as a function of a) J_1 for $\delta = 3$, b) J_1 for $\delta = 0$ and c) δ for $J_1 = 1$.

of wave transmission with $0.2 \lesssim J_1 \lesssim 0.8$. For larger J_1, the mean depth of the shear changes less from its initial position: wave emission becomes increasingly insignificant. However the extent of the mixing region increases dramatically. This occurs because the mixing region entrains increasingly dense fluid as J_1 increases and so mixing is enhanced by convection.

From simulations with $\delta = 0$, Fig. 5b similarly illustrates strong wave excitation made apparent by the large reduction in the mean depth of the shear layer at moderate values of J_1. Notably different in this case is the reduction in mixing for large J_1. In such cases, the stratified region immediately above the shear layer acts as a ceiling that significantly retards the growth rate of the most unstable mode.

Figure 5c shows that the proximity of the region of increased stratification to the shear layer is a crucial parameter in determining wave transmission. In simulations with $J_1 = 1$, transmission is greatest when the stratified layer immediately overlies the shear layer ($\delta = 0$). As δ increases, transmission decreases and mixing increases until $\delta \simeq 3$ at which point transmission increases again and mixing is reduced. This jump occurs as the instability mechanism switches from direct excitation by way of interaction with RI modes to indirect excitation by way of periodic flow over KH billows. For still larger δ transmission decreases until $\delta \gtrsim 9$ in which case transmission is negligibly small.

d Jet Flow Results

Here we extend the study of shear instability to that of an asymmetric jet whose unstable upper flank underlies a strongly stratified region and whose lower flank has sufficiently weak associated shear that it is stable in the sense that the gradient Richardson number is nowhere less than 1/4 across its span. The initial mean flow and squared buoyancy frequency profiles are given by (11) and (12), respectively, where now the jet-depth parameter, L_w, is a finite number. Length- and time-scales are once again set by the half-depth of the upper shear layer and its associated shear strength.

One reason to examine this more general circumstance is because the initial conditions more realistically represent the mean flow associated with a vertical cross-section through the Jet Stream as well as the stratification associated with the troposphere and lower stratosphere. The problem is of fundamental theoretical interest besides: new dynamics are introduced because the lower shear layer has a critical level associated with it, this being the height, z_l, at which the flow speed on the lower flank matches the flow speed at the height, z_u, at the midpoint of the upper shear layer. These are the two levels where the flow speed equals the phase speed of the most unstable mode. The simulation results reveal to what extent this lower critical layer acts as a vertical barrier to mixing and to momentum extraction by internal waves.

Figure 6 shows the end state of three jet-flow simulations. These are similar to the shear-flow results shown in Figure 3 except that here $L_w = 0$. An obvious difference between the two sets of results is the appearance of fine-scale structures in the jet-flow mixing region between the initial lower and upper critical layers at $z_l \equiv -6$ and $z_u \equiv 0$, respectively.

Although a coherent vortex is evident in the uniformly stratified case, Fig. 6a, its interaction with the lower critical layer results in the baroclinic generation of vortex filaments of positive and negative sign. As with the corresponding shear-flow case, negligible internal wave excitation occurs and so the evolution of the instability serves only to redistribute momentum locally about the upper flank of the jet. Though some momentum is extracted from the flow below the jet's initial lower critical level at z_l, the majority of the momentum transported across the

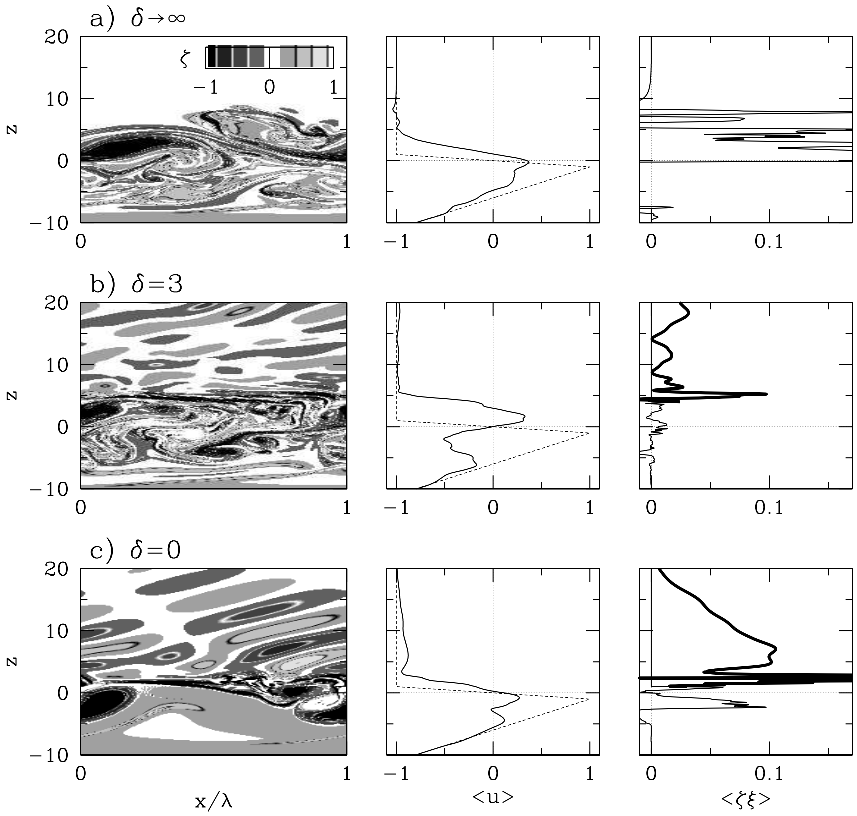

Figure 6: As in 3 but showing diagnostics at time $t = 100$ from simulated evolution of piecewise linear jet in a) uniform stratification $J_0 = 0.01$, and in nonuniform stratification with $J_0 = 0.01$ below $z = \delta$ and $J_1 = 1$ above $z = \delta$ in which b) $\delta = 3$ and c) $\delta = 0$.

upper flank of the jet is accounted for by the momentum extracted from the mixing region.

Even when internal wave excitation occurs in nonuniformly stratified flows, the jet's initial lower critical level continues to act as a partial barrier to momentum extraction. In the case with $\delta = 3$, shown in Fig. 6b, the mean flow below z_l varies relatively little from its initial profile although the flow decelerates substantially above this level within the mixing region. No single coherent vortex is evident in this case and, indeed, momentum transport across the upper flank of the jet is so strong that the shear at z_u changes sign and the mean flow develops the structure of a double jet.

In the case with $\delta = 0$, we see substantial deceleration of the jet in the mixing region above $z = z_l$. A significant fraction of this momentum loss is accounted for by wave radiation above the jet. As before the fluid below z_l decelerates negligibly. Thus the height $z = z_l$ acts similarly to a critical level even though the evolution of the mixing region is strongly nonlinear at late times.

A range of experiments have been performed to determine the relative momentum loss as a function of parameters J_1, δ and L_w. Figure 7 shows the results analogous to those in Fig. 5 but for the case $L_w = 0$. Also, rather than plotting $\Delta z_{\rm shr}$, here we plot the relative momentum loss due to waves $\Delta M/M_{\rm jet}$ in which ΔM is given by (14) and $M_{\rm jet} \equiv \int_{z_l}^{z_u} \bar{U}\, dz$ is the initial positive momentum per unit mass of the jet between the upper and lower critical layers.

Consistent with the shear flow simulations, for $\delta = 3$ and $\delta = 0$ we find that the greatest extraction of momentum by waves occurs for $J_1 \simeq 0.5$. The momentum extracted can be as large as 30 percent of the positive initial momentum of the jet. For $\delta = 0$, waves extract negligible momentum if $J_1 \gtrsim 4$, whereas wave emission is non-negligible for larger J_1 in simulations with $\delta = 3$.

Fixing $J_1 = 1$, Fig. 7c shows that, as in the case of the shear simulations, $\Delta M/M_{\rm jet}$ is large for $\delta = 0$ and is large again for moderately large $\delta \simeq 5$. In the former case wave emission is significant because of

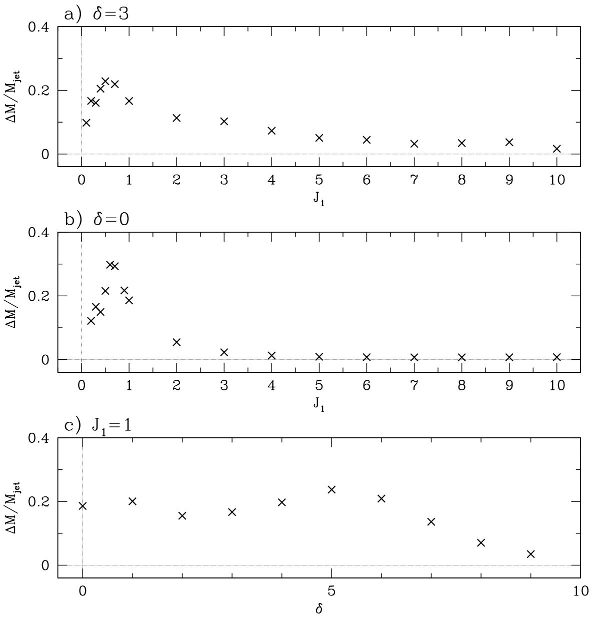

Figure 7: The relative momentum loss due to internal wave transmission from an unstable jet plotted as a function of a) J_1 for $\delta = 3$, b) J_1 for $\delta = 0$ and c) δ for $J_1 = 1$. In all cases $L_w = 0$ and $L_b = 5$.

interaction with RI modes; in the latter case wave emission is significant because KH billows indirectly excite radiating waves.

4 Discussion and Conclusions

We have examined the coupling between internal waves and Rayleigh waves in non-uniformly stratified fluid. Fully nonlinear numerical simulations reveal that this coupling is efficient at generating waves well beyond the linear regime. The efficiency is characterised by a new diagnostic developed from calculating the wave-induced mean flow (or pseudomomentum) associated with the transmitted waves. This analysis has the advantage in simulations that drag on a mixed region and momentum flux from it due to waves can be estimated instantaneously at a fixed time rather than time-integrating Reynolds stress at a fixed vertical level.

For a shear layer, internal wave excitation is strongest if $J_1 \simeq 0.5\,(\pm 0.3)$, in which J_1 is the external bulk Richarsdon number based on the far-field stratification and near-field maximum shear. Extraction of momentum by the waves is so large in such cases that the mean depth of the shear layer drops by the equivalent of the half depth of the initial shear layer. If the well stratified region lies immediately above the shear layer, direct internal wave excitation during the linear growth phase is the dominant mechanism for wave generation. One consequence of this is that, for large J_1, mixing in the shear layer during the nonlinear evolution of the flow is much weaker than in circumstances where the stratified region is far from the shear layer and internal waves are indirectly excited by way of flow over KH billows.

When strong wave excitation occurs the waves are excited with frequency approximately 0.4 of the maximum shear strength. For $J_1 \simeq 0.5\,(\pm 0.3)$, this frequency is close to but smaller than the far-field buoyancy frequency, N_1. From the dispersion relation of these non-hydrostatic internal waves, $\Omega = N_1 \cos\Theta = N_1 k/|\underline{k}|^2$, the angle between the vertical and lines of constant phase lies between $\Theta = 37^o$ and 62^o.

In simulations of an unstable jet flow, we likewise find strong wave excitation occurs if $J_1 \simeq 0.5\,(\pm 0.3)$ and we find mixing characteristics change depending on whether the wave excitation mechanism is direct or indirect.

The initial state of these simulations crudely represent a vertical cross section through the Jet Stream. Though it is uncertain how or even if the Jet Stream might evolve to such an unstable state, it is nonetheless instructive to examine the potential consequences for momentum transport into the stratosphere and for the concurrent drag on the mean flow of the Jet Stream itself.

We take $U_0 = 30\,\mathrm{m/s}$ and $L = 300\,\mathrm{m}$ to characterise the shear on the upper flank of a perturbed, unstable Jet Stream. In the stratosphere we suppose $N_1 = 10^{-2}\,\mathrm{s}^{-1}$ and that this enhanced stratification lies immediately above the shear layer. In terms of the nondimensional variables used in this study we have $J_1 = 1$ and $\delta = 0$. Here we suppose the stratification at the level of the shear is negligibly small, as characterised by setting the internal bulk Richardson number $J_0 = 0$. The simulation results predict that over a time of $100L/U_0 \simeq 17$ minutes the mean depth of the upper flank would drop by approximately $\Delta z_{\mathrm{shr}} \simeq 250\,\mathrm{m}$ as a result of drag due to wave excitation. In other words, over a depth of 250 m, the flow has decelerated at the enormous rate of 60 m/s in 17 minutes. Taking the density of air at the tropopause to be approximately $0.4\,\mathrm{kg/m^3}$ and using (19), the corresponding Reynolds stress due to wave emission is $6\,\mathrm{N/m^2}$ occurring on average throughout the mixed region over 17 minutes.

This is an extreme example. If instead we took the half-depth of the shear to be $L = 600\,\mathrm{m}$, then $J_1 = 4$, $\Delta z_{\mathrm{shr}} \simeq 20\,\mathrm{m}$ and the corresponding Reynolds stress would be $0.2\,\mathrm{N/m^2}$ over 33 minutes.

Mixing in a fully three dimensional flow would likely act to weaken wave excitation further. Such effects would be significant in large δ cases for which KH instability results in the development of vortex-braid structures and convective mixing (Peltier and Caulfield 2003). However, if the instability mechanism examined here occurs in reality, it is more likely it would occur due to the perturbation of a shear layer immediately underlying a stratified region, that is, for cases with $\delta \simeq 0$. The resulting coupling with RI modes excites waves without being mediated by the development of coherent vortices.

It would be useful to perform fully three-dimensional simulations that examine the coupling between internal waves and this sheared turbulent region. However, at this time such a numerical investigation would require prohibitively high resolution in the mixing region together with a spatial domain sufficiently large to allow for far-field wave propagation.

As well as the atmospheric application discussed above, the generic mechanism for wave excitation may be manifest in a variety of other geophysical circumstances. The equatorial undercurrent may be another example of realisable dynamic instability. The upper flank of this current lies in the proximity of the mixed region with an underlying strongly stratified thermocline, and significant turbulence and internal wave activity have been observed near the current (Moum, Caldwell and Paulson 1989, Peters, Gregg and Toole 1989). Although mechanisms for dynamic excitation have been explored (Sutherland 1996, Smyth and Moum 2002), more observations are required to determine the relative importance of this process compared with other wave generation mechanisms.

Acknowledgements

The author is grateful to the reviewers for suggestions that improved the linear theory analyses. This research was supported by the Canadian Foundation for Climate and Atmospheric Science (CFCAS).

REFERENCES

Alexander, M. J., J. R. Holton and D. R. Durran, 1995: The gravity wave response above deep convection in a squall line simulation. *J. Atmos. Sci.* **52**, 2212–2226.

Baines, P. G. and H. Mitsudera, 1994: On the mechanism of shear flow instabilities. *J. Fluid Mech.* **276**, 327–342.

Bühler, O., M. E. McIntyre and J. F. Scinocca, 1999: On shear-generated gravity waves that reach the mesosphere, Part I. Wave generation. *J. Atmos. Sci.* **56**, 3749–3763.

Caulfield, C. P., 1994: Multiple linear instability of layered stratified shear flow. *J. Fluid Mech.* **258**, 255–285.

Chimonas, G. and J. R. Grant, 1984: Shear excitation of gravity waves. Part II: Upscale scattering from Kelvin-Helmholtz waves. *J. Atmos. Sci.* **41**(15), 2278–2288.

Drazin, P. G. and L. N. Howard, 1966: Hydrodynamic stability of parallel flow of inviscid fluid. *Advances in Applied Mathematics* **9**, 1–89.

Drazin, P. G. and W. H. Reid, 1981: *Hydrodynamic Stability.* Cambridge University Press, Cambridge, England. 525 pp.

Fovell, R., D. Durran and J. R. Holton, 1992: Numerical simulations of convectively generated stratospheric gravity waves. *J. Atmos. Sci.* **49**(16), 1427–1442.

Fritts, D. C., 1984: Shear excitation of atmospheric gravity waves. Part II: Nonlinear radiation from a free shear layer. *J. Atmos. Sci.* **41**(4), 524–537.

Fritts, D. C. and G. D. Nastrom, 1992: Sources of mesoscale variability of gravity waves. Part II: Frontal, convective, and jet stream excitation. *J. Atmos. Sci.* **49**, 111–127.

Herron, T. J. and I. Tolstoy, 1969: Tracking jet stream winds from ground level pressure signals. *J. Atmos. Sci.* **26**, 266–269.

Howard, L. N., 1961: Note on a paper by John W. Miles. *J. Fluid Mech.* **10**, 509–512.

Keliher, T. E., 1975: The occurrence of microbarograph-detected gravity waves compared with the existence of dynamically unstable wind shear layers. *J. Geophys. Res.* **80**, 2967–2976.

Klaassen, G. P. and W. R. Peltier, 1985: The onset of turbulence in finite-amplitude Kelvin-Helmholtz billows. *J. Fluid Mech.* **155**, 1–35.

Lindzen, R. S., 1974: Stability of a Helmholtz velocity profile in a continuously stratified infinite Boussinesq fluid – applications to clear air turbulence. *J. Atmos. Sci.* **31**, 1507–1514.

Lindzen, R. S. and A. J. Rosenthal, 1976: On the instability of Helmholtz velocity profiles in stably stratified fluids when a lower boundary is present. *J. Geophys. Res.* **81**(9), 1561–1571.

Miles, J. W., 1961: On the stability of heterogeneous shear flows. *J. Fluid Mech.* **10**, 496–508.

Moum, J. N., D. R. Caldwell and C. A. Paulson, 1989: Mixing in the equatorial surface layer and thermocline. *J. Geophys. Res.* **94**, 2005–2021.

Peltier, W. R. and C. P. Caulfield, 2003: Mixing efficiency in stratified shear flows. *Annu. Rev. Fluid Mech.* **35**, 135–167.

Peters, H., M. C. Gregg and J. Toole, 1989: Meridional variability of turbulence through the equatorial undercurrent. *J. Geophys. Res.* **94**, 18003–18009.

Scinocca, J. F. and R. Ford, 2000: The nonlinear forcing of large-scale internal gravity waves by stratified shear instability. *J. Atmos. Sci.* **57**, 653–672.

Scinocca, J. F. and T. G. Shepherd, 1992: Nonlinear wave-activity conservation laws and Hamiltonian structure for the two-dimensional anelastic equations. *J. Atmos. Sci.* **49**, 5–27.

Scorer, R. S., 1949: Theory of waves in the lee of mountains. *Quart. J. Roy. Meteor. Soc.* **75**, 41–56.

Smyth, W. D. and J. N. Moum, 2002: Shear instability and gravity wave saturation in an asymmetrically stratified jet. *Dyn. Atmos. Oceans* **35**(3), 265–294.

Snively, J. B. and V. P. Pasko, 2003: Breaking of thunderstorm-generated gravity waves as a source of short-period ducted waves at mesopause altitudes. *Geophys. Res. Lett.* **30**(24), 2254.

Sutherland, B. R., 1996: The dynamic excitation of internal gravity waves in the equatorial oceans. *J. Phys. Oceanogr.* **26**, 3214–3235.

Sutherland, B. R., 1999: Propagation and reflection of large amplitude internal gravity waves. *Phys. Fluids* **11**, 1081–1090.

Sutherland, B. R., 2001: Finite-amplitude internal wavepacket dispersion and breaking. *J. Fluid Mech.* **429**, 343–380.

Sutherland, B. R., C. P. Caulfield and W. R. Peltier, 1994: Internal wave generation and hydrodynamic instability. *J. Atmos. Sci.* **51**, 3261–3280.

Sutherland, B. R. and W. R. Peltier, 1994: Turbulence transition and internal wave generation in density stratified jets. *Phys. Fluids A* **6**, 1267–1284.

Sutherland, B. R. and W. R. Peltier, 1995: Internal gravity wave emission into the middle atmosphere from a model tropospheric jet. *J. Atmos. Sci.* **52**, 3214–3235.

Tse, K. L., A. Mahalov, B. Nicolaenko and H. J. S. Fernando, 2003: Quasi-equilibrium dynamics of shear-stratified turbulence in a model tropospheric jet. *J. Fluid Mech.* **496**, 73–103.

Vadas, S. L. and D. C. Fritts, 2001: Gravity wave radiation and mean responses to local body forces in the atmosphere. *J. Atmos. Sci.* **58**, 2249–2279.

Walterscheid, R. L., G. Schubert and D. G. Brinkman, 2001: Small-scale gravity waves in the upper mesosphere and lower thermosphere generated by deep tropical convection. *J. Geophys. Res.* **106**(D23), 31825–31832.